Mon. Not. R. Astron. Soc. **384,** 834–842 (2008) doi:10.1111/j.1365-2966.2007.12771.x

Exact general relativistic discs and the advance of perihelion

D. Vogt★ and P. S. Letelier★

Departamento de Matemática Aplicada-IMECC, Universidade Estadual de Campinas 13083-970 Campinas, SP, Brazil

Accepted 2007 November 23. Received 2007 November 22; in original form 2007 October 10

ABSTRACT

The advance of perihelion for geodesic motion on the galactic plane of some exact general relativistic disc solutions is calculated. Approximate analytical and numerical results are presented for the static Chazy–Curzon and the Schwarzschild discs in Weyl coordinates, the Schwarzschild disc in isotropic coordinates and the stationary Kerr disc in the Weyl–Lewis–Papapetrou metrics. It is found that for these disc models the advance of perihelion may be an increasing or decreasing function of the orbital excentricity. The precession due to Newtonian gravity for these disc models is also calculated.

Key words: relativity – stellar dynamics – celestial mechanics – galaxies: kinematics and dynamics.

1 INTRODUCTION

The explanation of the anomalous precession of Mercury's orbit by Einstein in 1915 was one of the first successful predictions of general relativity. In recent times the subject has received considerable attention with the possibility of high-precision measurements of general relativistic effects in the orbits of binary pulsars like the PSR 1913+16 system discovered in 1974 (Hulse & Taylor 1975). Schäfer & Damour (1988) discuss in-depth higher order general relativistic contributions to the periastron advance of binary pulsars. Schäfer & Wex (1993) calculated the periastron advance for a system composed of a Kerr black hole and an orbiting star.

In the context of axially symmetric solutions of Einstein vacuum equations, Boisseau & Letelier (2002) calculated the effect of different general relativistic multipole expansions in the advance of perihelion of test particles orbiting static axially symmetric attraction centres. Bini et al. (2005) derived approximate expressions for the periastron shift for motion in static and stationary axially symmetric space–times. However, we did not find in the literature similar works for general relativistic solutions with matter, in particular, disc-like configurations. Several such solutions can be found in the literature, e.g. Morgan & Morgan (1969), Bardeen & Wagoner (1971), Lynden-Bell & Pineault (1978), Chamorro, Gregory & Stewart (1987), Lemos (1989), Bičák & Ledvinka (1993), Bičák, Lynden-Bell & Pichon (1993b), Lemos & Letelier (1994), Neugebauer & Meinel (1995), Pichon & Lynden-Bell (1996) and González & Espitia (2003).

The aim of this work is to study the advance of perihelion for motion of test particles in the galactic plane for a few exact solutions of Einstein field equations that represent disc-like configurations of matter (Bičák, Lynden-Bell & Katz 1993a; González & Letelier 2000; Vogt & Letelier 2003; González & Letelier 2004; Vogt & Letelier 2005a,b). We derive approximate expressions and also present numerical results. We find that when matter is present the periastron shift may be an increasing or a decreasing function of the orbital excentricity. The paper is divided as follows. In Section 2 we present the formalism to calculate the periastron shift for relativistic elliptic orbits of test particles. This formalism is then applied in Section 3 to two exact models of static relativistic discs in canonical Weyl coordinates and to one solution expressed in isotropic coordinates. In Section 4 we calculate the periastron shift for a solution of a rotating disc obtained from the Kerr metric. In Section 5 we calculate the contribution of Newtonian gravity to the precession in the presented disc models so that it can be separated from relativistic effects. Finally, in Section 6 we present a short discussion of the results. Along the work we take units such that $c = G = 1$.

2 ADVANCE OF THE PERIHELION IN RELATIVISTIC ORBITS

In this section we derive the formulae to calculate the advance of perihelion for geodesic elliptic-like orbits in an axial symmetric space–time with cylindrical coordinates (t, r, z, φ). We follow closely Bini et al. (2005). Let us assume a test particle is bound in an elliptic orbit on the plane $z = 0$. This orbit can be parametrized as

$$r = \frac{d(1 - e^2)}{1 + e\cos\chi}, \tag{1}$$

★E-mail: dvogt@ime.unicamp.br (DV); letelier@ime.unicamp.br (PSL)

where d and e are, respectively, the ellipse's semimajor axis and excentricity, and χ is a variable called relativistic anomaly. From equation (1) we see that the minimum value $r_{\rm m} = d(1-e)$ is obtained for $\chi = 0$ and the maximum value $r_{\rm p} = d(1+e)$ when $\chi = \pi$. At these points the equation $\mathrm{d}r/\mathrm{d}\varphi$ that describes the shape of the orbit vanishes. The relation between the functions φ e χ can be expressed as

$$\frac{\mathrm{d}\varphi}{\mathrm{d}\chi} = \frac{ed(1-e^2)\sin\chi}{(1+e\cos\chi)^2}\left.\frac{\mathrm{d}\varphi}{\mathrm{d}r}\right|_{r=r(\chi)}, \tag{2}$$

where equation (1) was used. By symmetry, the change in the coordinate φ when χ decreases from π to 0 is the same that when χ increases from 0 to π; thus the total change in the coordinate φ in one revolution is $2[\varphi(\pi) - \varphi(0)]$, where

$$\varphi(\pi) - \varphi(0) = \int_0^{\pi} \frac{ed(1-e^2)\sin\chi}{(1+e\cos\chi)^2}\left.\frac{\mathrm{d}\varphi}{\mathrm{d}r}\right|_{r=r(\chi)} \mathrm{d}\chi. \tag{3}$$

In a closed ellipse φ would change by 2π per revolution, so the orbit precesses by an angle

$$\Delta\varphi = 2[\varphi(\pi) - \varphi(0)] - 2\pi \tag{4}$$

in one revolution. In general it is not possible to express the integral equation (3) in terms of elementary functions; we will evaluate it numerically and also derive approximate expressions.

3 ADVANCE OF THE PERIHELION AND STATIC RELATIVISTIC DISCS

We study first the precession of perihelion for orbits in static relativistic disc models in Weyl coordinates and isotropic coordinates.

3.1 Weyl coordinates

The general metric for a static axially symmetric space–time in Weyl's canonical coordinates (t, r, z, φ) is given by

$$\mathrm{d}s^2 = -\mathrm{e}^{2\Phi}\mathrm{d}t^2 + \mathrm{e}^{-2\Phi}[\mathrm{e}^{2\Lambda}(\mathrm{d}r^2 + \mathrm{d}z^2) + r^2\mathrm{d}\varphi^2], \tag{5}$$

where Φ and Λ are functions of r and z. The Einstein vacuum equations for this metric reduce to the Weyl equations (Weyl 1917, 1919)

$$\Phi_{,rr} + \frac{\Phi_r}{r} + \Phi_{,zz} = 0, \tag{6}$$

$$\Lambda_r = r\left(\Phi_r^2 - \Phi_z^2\right), \qquad \Lambda_z = 2r\Phi_r\Phi_z. \tag{7}$$

We shall consider two solutions of equations (6) and (7): the Chazy–Curzon solution (Chazy 1924; Curzon 1924)

$$\mathrm{e}^{2\Phi} = \mathrm{e}^{-2m/R}, \qquad \mathrm{e}^{2\Lambda} = \mathrm{e}^{-m^2r^2/R^4}, \tag{8}$$

where $R = \sqrt{r^2+z^2}$, and the Schwarzschild solution, expressed as (Weyl 1917)

$$\Phi = \frac{1}{2}\ln\left[\frac{R_1+R_2-2m}{R_1+R_2+2m}\right], \quad \Lambda = \frac{1}{2}\ln\left[\frac{(R_1+R_2)^2-4m^2}{4R_1R_2}\right], \tag{9}$$

with $R_1^2 = r^2 + (m+z)^2$, $R_2^2 = r^2 + (-m+z)^2$.

Let us briefly recall a procedure to generate disc-like distributions of matter given a vacuum solution of Einstein field equations. Mathematically, it consists in applying a transformation $z \to \mathrm{h}(z) + a$ on a given vacuum solution and then calculate the resulting energy–momentum tensor using Einstein's field equations. Thin discs can be obtained if we choose $\mathrm{h} = |z|$. For instance, Bičák et al. (1993a) constructed thin discs using the Curzon solution equation (8) and the Schwarzschild solution equation (9). On the other hand, thick discs can be constructed starting with the same vacuum solutions and using a class of even polynomials for $\mathrm{h}(z)$; see González & Letelier (2004) and Vogt & Letelier (2005a) for details. Also, a transformation originally proposed by Miyamoto & Nagai (1975) with $\mathrm{h}(z) = \sqrt{z^2+b^2}$ was used by Vogt & Letelier (2005b) to generate relativistic disc-like distributions of matter from the Schwarzschild vacuum solution in isotropic coordinates. For our analysis, the advance of perihelion is always calculated on the galactic plane $z = 0$, where all the above mentioned transformations reduce to a constant. Thus, the results apply equally to thin and to thick discs. Henceforth this constant will be denoted a.

For time-like orbits on the $z = 0$ plane, the Lagrangian associated to metric equation (5) reads

$$2\mathcal{L} = -1 = -\mathrm{e}^{2\Phi}\dot{t}^2 + \mathrm{e}^{2(\Lambda-\Phi)}\dot{r}^2 + r^2\mathrm{e}^{-2\Phi}\dot{\varphi}^2, \tag{10}$$

where dots indicate differentiation with respect to proper time. Due to the independence of $\mathcal{L}$ from t e φ, the conserved energy E and angular momentum h per unit mass can be introduced:

$$E = \mathrm{e}^{2\Phi}\dot{t}, \qquad h = r^2\mathrm{e}^{-2\Phi}\dot{\varphi}. \tag{11}$$

Using equation (11), the expression for the shape of the orbit follows from equation (10):

$$\frac{\mathrm{d}r}{\mathrm{d}\varphi} = \frac{r}{\mathrm{e}^{\Lambda}}\left[\frac{r^2\mathrm{e}^{-2\Phi}(E^2\mathrm{e}^{-2\Phi}-1)}{h^2} - 1\right]^{1/2}. \tag{12}$$

For an elliptic orbit with excentricity e and semimajor axis d, the two constants of motion can be calculated by substituting $r_{\rm m} = d(1-e)$ and $r_{\rm p} = d(1+e)$ in $\mathrm{d}r/\mathrm{d}\varphi = 0$ and solving the system. We have

$$E^2 = \frac{r_{\rm p}^2 \mathrm{e}^{-2\Phi_{\rm p}} - r_{\rm m}^2 \mathrm{e}^{-2\Phi_{\rm m}}}{r_{\rm p}^2 \mathrm{e}^{-4\Phi_{\rm p}} - r_{\rm m}^2 \mathrm{e}^{-4\Phi_{\rm m}}}, \qquad h^2 = \frac{r_{\rm p}^2 r_{\rm m}^2 \mathrm{e}^{-2(\Phi_{\rm p}+\Phi_{\rm m})}\left(\mathrm{e}^{-2\Phi_{\rm m}} - \mathrm{e}^{-2\Phi_{\rm p}}\right)}{r_{\rm p}^2 \mathrm{e}^{-4\Phi_{\rm p}} - r_{\rm m}^2 \mathrm{e}^{-4\Phi_{\rm m}}}, \tag{13}$$

where $\Phi_{\rm m} = \Phi(r_{\rm m})$ and $\Phi_{\rm p} = \Phi(r_{\rm p})$.

To estimate the advance of perihelion for orbits in the $z = 0$ plane for both disc models, it is reasonable to suppose that m/d and a/d are small quantities and expand equation (3) with equations (12)–(13) in multivariate Taylor series. For the Curzon disc, the expansion up to third order reads

$$\Delta\varphi = \frac{6\pi m}{d(1-e^2)} - \frac{3\pi a^2}{d^2(1-e^2)^2} + \frac{\pi m^2(44-9e^2)}{2d^2(1-e^2)^2} - \frac{6\pi m a^2(6+e^2)}{d^3(1-e^2)^3} + \frac{\pi m^3(192-53e^2)}{2d^3(1-e^2)^3}, \tag{14}$$

while for the Schwarzschild disc we obtain

$$\Delta\varphi = \frac{6\pi m}{d(1-e^2)} - \frac{3\pi a^2}{d^2(1-e^2)^2} + \frac{3\pi m^2(14-3e^2)}{2d^2(1-e^2)^2} - \frac{6\pi m a^2(6+e^2)}{d^3(1-e^2)^3} + \frac{3\pi m^3(56-19e^2)}{2d^3(1-e^2)^3}. \tag{15}$$

Both expansions with $a = 0$ agree with those presented by Bini et al. (2005) up to second order. In equations (14) and (15) the terms corresponding to the vacuum solutions are all positive, whereas the ones related to the presence of matter (parameter a) have negative signs. When matter is absent, the angle of advance is an increasing function with respect to excentricity, but expansions (14) and (15) suggest that this may not be true in the present disc models. By imposing $\partial(\Delta\varphi)/\partial e = 0$ in equations (14) and (15), the following expressions for the parameter a are obtained, respectively,

$$a^2 = \frac{m[12d^2(1-e^2)^2 + md(1-e^2)(79-9e^2) + m^2(523-106e^2)]}{12[d(1-e^2) + m(19+2e^2)]}, \tag{16}$$

$$a^2 = \frac{m[4d^2(1-e^2)^2 + md(1-e^2)(25-3e^2) + m^2(149-38e^2)]}{4[d(1-e^2) + m(19+2e^2)]}. \tag{17}$$

These expressions, evaluated for $e = 0$ and 1, yield the results

$$a^2 = \frac{m(12d^2 + 79md + 523m^2)}{12(d+19m)}, \quad a^2 = \frac{139m^2}{84} \quad \text{(Curzon)}, \tag{18}$$

$$a^2 = \frac{m(4d^2 + 25md + 149m^2)}{4(d+19m)}, \quad a^2 = \frac{37m^2}{28} \quad \text{(Schwarzschild)}. \tag{19}$$

Equations (18) and (19) give an estimate for the ranges in the parameter a for which the angle of advance as a function of excentricity has a critical point.

Figs 1(a)–(c) show the angle of precession as function of excentricity for the Chazy–Curzon disc with parameters $m/d = 0.01$, $a/d = 0.05$ in Fig. 1(a), $a/d = 0.075$ in (b) and $a/d = 0.1$ in (c). The curves with solid lines were calculated by numerical integration of equation (3), those with dashed lines represent expansion equation (14) with terms up to second order, and the dotted lines the same expression but with terms of third order. Figs 2(a)–(c) show the results for the Schwarzschild disc with the same value of parameters. In both cases the numerical results and the expansion up to third order agree well for small values of e. Using the estimates given by equations (18) and (19), the intervals with critical points would be $0.0128 \leqslant a/d \leqslant 0.0948$ and $0.0115 \leqslant a/d \leqslant 0.0946$, respectively.

3.2 Isotropic coordinates

The line element in isotropic form in cylindrical coordinates (t, r, z, φ) may be expressed as

$$\mathrm{d}s^2 = -\mathrm{e}^{2\Phi}\mathrm{d}t^2 + \mathrm{e}^{2\Lambda}(\mathrm{d}r^2 + \mathrm{d}z^2 + r^2\mathrm{d}\varphi^2), \tag{20}$$

where the Φ and Λ are only functions of r and z. The vacuum Schwarzschild solution for metric equation (20) has the form

$$\mathrm{e}^{2\Phi} = \left[\frac{1-m/(2R)}{1+m/(2R)}\right]^2, \qquad \mathrm{e}^{2\Lambda} = \left(1+\frac{m}{2R}\right)^4, \tag{21}$$

where $R = \sqrt{r^2+z^2}$. Also here disc-like distributions of matter can be generated by applying convenient transformations on the z coordinate (see e.g. Vogt & Letelier 2003; González & Letelier 2004; Vogt & Letelier 2005a,b), as was discussed in Section 3.1.

For metric equation (20), the shape of the orbit of a test particle confined on the $z = 0$ plane is described by

$$\frac{\mathrm{d}r}{\mathrm{d}\varphi} = r\left[\frac{r^2\mathrm{e}^{2\Lambda}(E^2\mathrm{e}^{-2\Phi}-1)}{h^2} - 1\right]^{1/2}. \tag{22}$$

The constants of motion E and h are now given by the following expressions:

$$E^2 = \frac{r_{\rm p}^2 \mathrm{e}^{2\Lambda_{\rm p}} - r_{\rm m}^2 \mathrm{e}^{2\Lambda_{\rm m}}}{r_{\rm p}^2 \mathrm{e}^{2(\Lambda_{\rm p}-\Phi_{\rm p})} - r_{\rm m}^2 \mathrm{e}^{2(\Lambda_{\rm m}-\Phi_{\rm m})}}, \qquad h^2 = \frac{r_{\rm p}^2 r_{\rm m}^2 \mathrm{e}^{2(\Lambda_{\rm p}+\Lambda_{\rm m})}(\mathrm{e}^{-2\Phi_{\rm m}} - \mathrm{e}^{-2\Phi_{\rm p}})}{r_{\rm p}^2 \mathrm{e}^{2(\Lambda_{\rm p}-\Phi_{\rm p})} - r_{\rm m}^2 \mathrm{e}^{2(\Lambda_{\rm m}-\Phi_{\rm m})}}, \tag{23}$$

with the same notation as defined in Section 3.1.

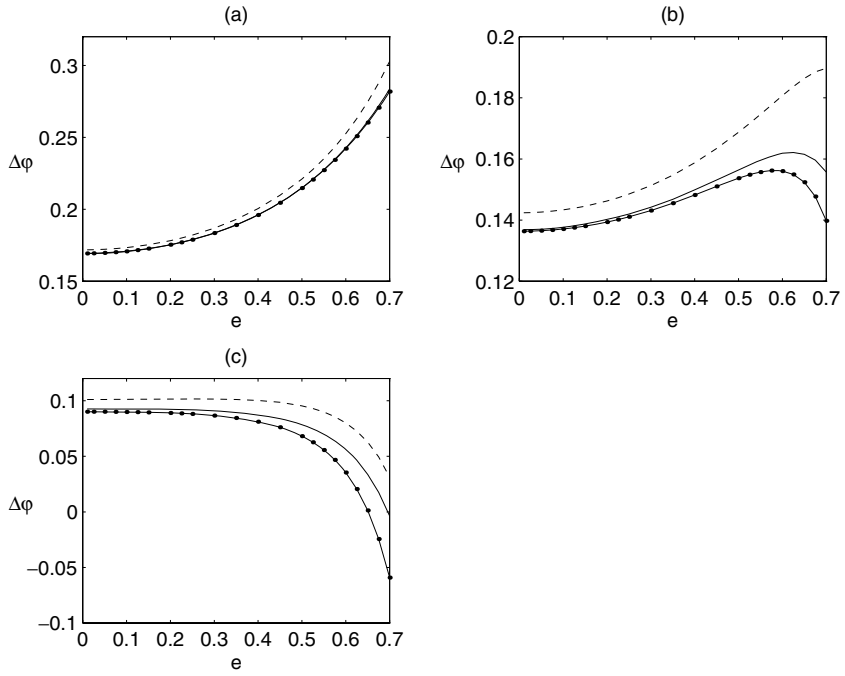

Figure 1. The advance of the perihelion $\Delta\varphi$ as function of excentricity e for the Chazy–Curzon disc. Parameters: $m/d = 0.01$, $a/d = 0.05$ in (a), $a/d = 0.075$ in (b) and $a/d = 0.1$ in (c). Solid lines: numerical integration of equation (3). Dashed lines: values obtained from equation (14) up to terms of second order. Dotted lines: the same expansion with terms of third order.

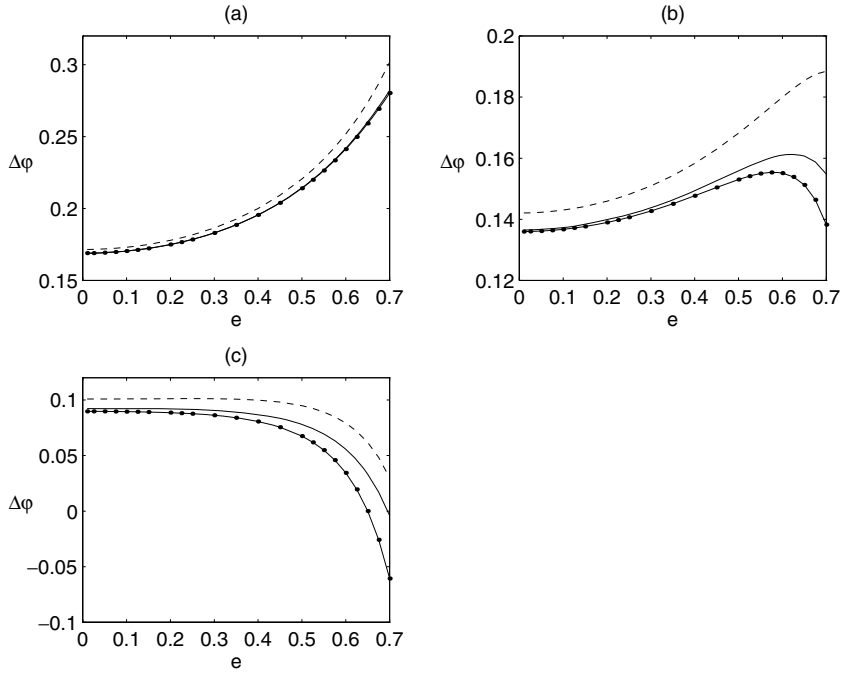

Figure 2. The perihelion shift $\Delta\varphi$ as function of excentricity e for the Schwarzschild disc. Parameters: $m/d = 0.01$, $a/d = 0.05$ in (a), $a/d = 0.075$ in (b) and $a/d = 0.1$ in (c). Solid lines: numerical integration of equation (3). Dashed lines: values obtained from equation (15) up to terms of second order. Dotted lines: the same expansion with terms of third order.

For the Schwarzschild disc in isotropic coordinates, an approximate expression for the precession of perihelion reads

$$\Delta\varphi = \frac{6\pi m}{d(1-e^2)} - \frac{3\pi a^2}{d^2(1-e^2)^2} + \frac{3\pi m^2(14-3e^2)}{2d^2(1-e^2)^2} - \frac{6\pi m a^2(6+e^2)}{d^3(1-e^2)^3} + \frac{3\pi m^3(57-16e^2)}{2d^3(1-e^2)^3}. \tag{24}$$

Comparing equations (15) and (24) reveals that they are almost identical, the difference beginning only in the last term. The calculation of $\partial(\Delta\varphi)/\partial e = 0$ provides

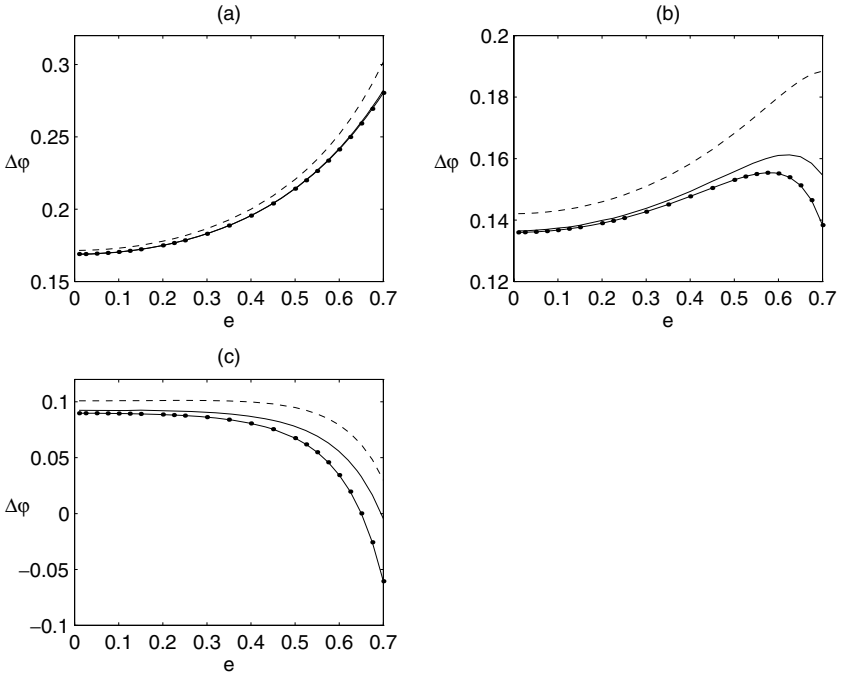

Figure 3. The advance of the perihelion $\Delta\varphi$ as function of excentricity e for the Schwarzschild disc in isotropic coordinates. Parameters: $m/d = 0.01$, $a/d = 0.05$ in (a), $a/d = 0.075$ in (b) and $a/d = 0.1$ in (c). Solid lines: numerical integration of equation (3). Dashed lines: values obtained from equation (24) up to terms of second order. Dotted lines: the same expansion with terms of third order.

$$a^2 = \frac{m[4d^2(1-e^2)^2 + md(1-e^2)(25-3e^2) + m^2(155-32e^2)]}{4[d(1-e^2) + m(19+2e^2)]}, \tag{25}$$

which evaluated on $e = 0$ and 1 gives, respectively,

$$a^2 = \frac{m(4d^2 + 25md + 155m^2)}{4(d+19m)}, \quad a^2 = \frac{41m^2}{28}. \tag{26}$$

Figs 3(a)–(c) display some curves of the angle $\Delta\varphi$ as function of the excentricity e for the Schwarzschild disc in isotropic coordinates with parameters $m/d = 0.01$, $a/d = 0.05$ in Fig. 3(a), $a/d = 0.075$ in Fig. 3(b) and $a/d = 0.1$ in Fig. 3(c). The curves with solid lines were calculated by numerical integration of equation (3), those with dashed lines represent expansion equation (24) with terms up to second order, and the dotted lines the same expression but with terms of third order. For this example, equation (26) estimate an interval $0.0121 \leqslant a/d \leqslant 0.0947$. Finally in Figs 4(a)–(c) the three disc models are compared. The parameters taken were $m/d = 0.15$ and $a/d = 0.175$ in Fig. 4(a), $a/d = 0.225$ in Fig. 4(b) and $a/d = 0.275$ in Fig. 4(c). All curves were obtained by numerical integration of equation (3). Solid lines represent the results for the Chazy–Curzon disc, dashed lines for the Schwarzschild disc in Weyl coordinates and dotted lines for the Schwarzschild disc in isotropic coordinates. Remember that as the parameter a is increased, all the discs become less relativistic (Bičák et al. 1993a; Vogt & Letelier 2003). This is reflected in the numerical values of the precession angle, which are greater in Fig. 4(a) than in Fig. 4(c). Qualitatively the curves for the three disc models are similar. As suggested by the expansions equations (15) and (24), both models obtained from the Schwarzschild solution give quite similar results for low excentric orbits.

4 ADVANCE OF THE PERIHELION AND STATIONARY RELATIVISTIC DISCS

In this section we investigate the effect of rotation on the perihelion shift for stationary relativistic discs, in particular discs generated from the vacuum Kerr metric. We begin with the metric for a stationary axially symmetric space–time

$$ds^2 = -e^{2\Phi}(dt + \mathcal{A}d\varphi)^2 + e^{-2\Phi}[r^2 d\varphi^2 + e^{2\Lambda}(dr^2 + dz^2)], \tag{27}$$

where Φ, Λ and $\mathcal{A}$ are functions of r and z. The vacuum Kerr solution for metric equation (27) may be written as

$$\Phi = \frac{1}{2}\ln\left[\frac{(R_1+R_2)^2 - 4m^2 + \alpha^2(R_1-R_2)^2/\sigma^2}{(R_1+R_2+2m)^2 + \alpha^2(R_1-R_2)^2/\sigma^2}\right], \tag{28}$$

$$\Lambda = \frac{1}{2}\ln\left[\frac{(R_1+R_2)^2 - 4m^2 + \alpha^2(R_1-R_2)^2/\sigma^2}{4R_1R_2}\right], \tag{29}$$

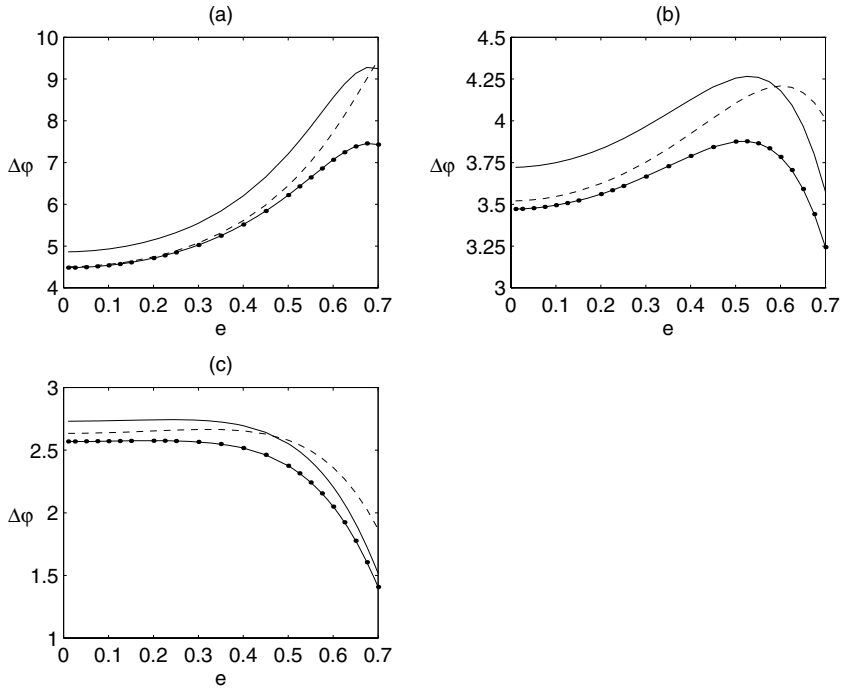

Figure 4. The advance of the perihelion $\Delta\varphi$ as function of excentricity e for the three disc models. Parameters: $m/d = 0.15$, $a/d = 0.175$ in (a), $a/d = 0.225$ in (b) and $a/d = 0.275$ in (c). Solid lines: Chazy–Curzon disc. Dashed lines: Schwarzschild disc in Weyl coordinates. Dotted lines: Schwarzschild disc in isotropic coordinates.

$$\mathcal{A} = \frac{\alpha m}{\sigma^2}\frac{(R_1+R_2+2m)\left[4\sigma^2-(R_1-R_2)^2\right]}{(R_1+R_2)^2-4m^2+\alpha^2(R_1-R_2)^2/\sigma^2}, \tag{30}$$

where m and α are, respectively, the mass and the Kerr parameter, $R_1 = \sqrt{r^2+(z+\sigma)^2}$, $R_2 = \sqrt{r^2+(z-\sigma)^2}$ and $\sigma = \sqrt{m^2-\alpha^2}$. Following the same procedure taken in Section 3, the orbit's shape of a test particle on the plane $z = 0$ for metric equation (27) is described by

$$\frac{\mathrm{d}r}{\mathrm{d}\varphi} = \frac{r}{\mathrm{e}^{\Lambda}}\left[\frac{r^2\mathrm{e}^{-2\Phi}(E^2\mathrm{e}^{-2\Phi}-1)}{(E\mathcal{A}+h)^2}-1\right]^{1/2}. \tag{31}$$

The conserved energy E and angular momentum h are found by solving the system of equations

$$r_{\mathrm{p}}^2\mathrm{e}^{-2\Phi_{\mathrm{p}}}(E^2\mathrm{e}^{-2\Phi_{\mathrm{p}}}-1)-(E\mathcal{A}_{\mathrm{p}}+h)^2 = 0, \tag{32}$$

$$r_{\mathrm{m}}^2\mathrm{e}^{-2\Phi_{\mathrm{m}}}(E^2\mathrm{e}^{-2\Phi_{\mathrm{m}}}-1)-(E\mathcal{A}_{\mathrm{m}}+h)^2 = 0, \tag{33}$$

where $\mathcal{A}_{\mathrm{p}} = \mathcal{A}(r_{\mathrm{p}})$, $\mathcal{A}_{\mathrm{m}} = \mathcal{A}(r_{\mathrm{m}})$, and where again the same notation was used as defined in Section 3.1. For a given excentricity e and semimajor axis d the system of equations admits two distinct solutions, corresponding to prograde ($h > 0$) and retrograde ($h < 0$) orbits. After applying a convenient transformation on the Kerr solutions (28)–(30) to generate stationary disc-like distributions of matter (see González & Letelier 2000; Vogt & Letelier 2007), we assume the ratios m/d, a/d and α/d to be small and expand equation (3) in series up to third order[1]:

$$\begin{aligned}\Delta\varphi = {} & \frac{6\pi m}{d(1-e^2)} \mp \frac{8\pi\alpha m^{1/2}}{d^{3/2}(1-e^2)^{3/2}} - \frac{3\pi a^2}{d^2(1-e^2)^2} + \frac{3\pi m^2(14-3e^2)}{2d^2(1-e^2)^2} + \frac{3\pi\alpha^2}{d^2(1-e^2)^2} \mp \frac{12\pi\alpha m^{3/2}(5-e^2)}{d^{5/2}(1-e^2)^{5/2}} \\ & - \frac{6\pi m a^2(6+e^2)}{d^3(1-e^2)^3} + \frac{3\pi m^3(56-19e^2)}{2d^3(1-e^2)^3} + \frac{6\pi m\alpha^2(12-e^2)}{d^3(1-e^2)^3},\end{aligned} \tag{34}$$

where the minus (plus) sign refers to prograde (retrograde) orbits. The solution of $\partial\,(\Delta\varphi)/\partial\, e = 0$ yields

$$\begin{aligned}a^2 = {} & \frac{1}{4[d(1-e^2)+m(19+2e^2)]}\{m[4d^2(1-e^2)^2+md(1-e^2)(25-3e^2)+m^2(149-38e^2)+4\alpha^2(35-2e^2)] \\ & + 4\alpha d^{1/2}(1-e^2)^{1/2}[\alpha d^{1/2}(1-e^2)^{1/2} \mp 2m^{1/2}d(1-e^2) \mp m^{3/2}(23-3e^2)]\},\end{aligned} \tag{35}$$

which for $e = 0$ and 1 simplifies to

$$a^2 = \frac{m(4d^2+25md+149m^2+140\alpha^2)+4\alpha d^{1/2}(\alpha d^{1/2} \mp 2m^{1/2}d \mp 23m^{3/2})}{4(d+19m)}, \tag{36}$$

[1] There is a discrepancy of a factor of 2 between our result and the second term of equation (34) in Bini et al. (2005). We compared both expressions with the numerical integration of the exact expressions for vacuum and our result is closer to the numerical values.

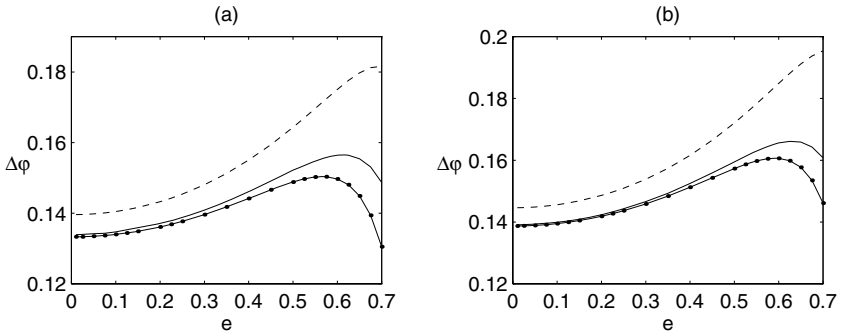

Figure 5. The perihelion shift $\Delta\varphi$ as function of excentricity e for the Kerr disc. Parameters: $m/d = 0.01$, $a/d = 0.075$ and $\alpha/d = 0.001$. Fig. 5(a) displays results for prograde orbits and (b) for retrograde orbits. Solid lines: numerical integration of equation (3). Dashed lines: values obtained from equation (34) up to terms of second order. Dotted lines: the same expansion with terms of third order.

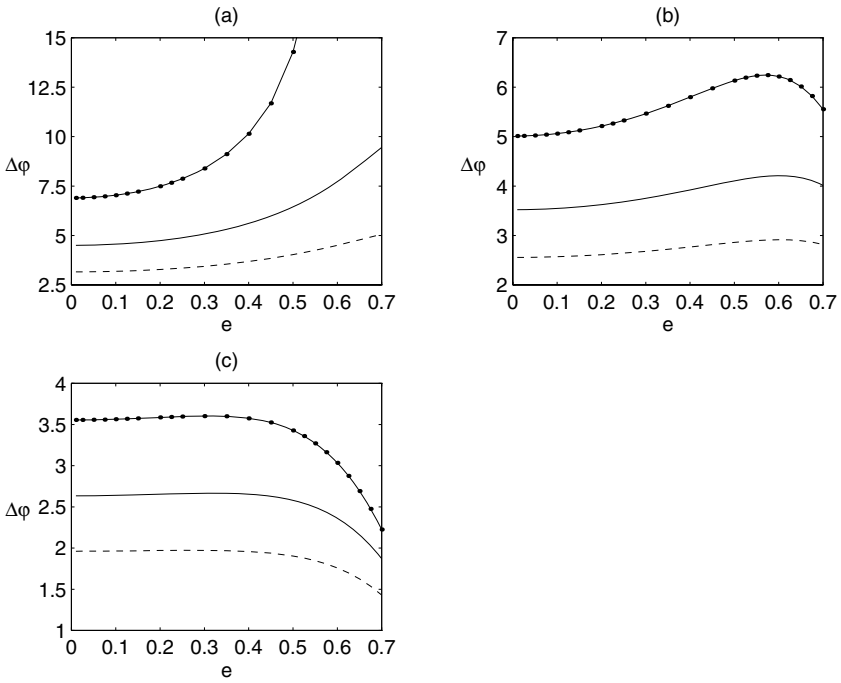

Figure 6. The perihelion shift $\Delta\varphi$ as function of excentricity e for the Kerr disc. Parameters: $m/d = 0.15$, $\alpha/d = 0.05$, $a/d = 0.175$ in (a), $a/d = 0.225$ in (b) and $a/d = 0.275$ in (c). Solid lines: disc without rotation. Dashed lines: prograde orbits. Dotted lines: retrograde orbits.

$$a^2 = \frac{37m^2 + 44\alpha^2}{28}, \tag{37}$$

respectively.

Figs 5(a)–(b) show the advance of the perihelion as function of excentricity for the Kerr disc with parameters $m/d = 0.01$, $a/d = 0.075$ and $\alpha/d = 0.001$. The curves in Fig. 5(a) are the results for prograde orbits and Fig. 5(b) for retrograde orbits. Curves with solid lines were calculated by numerical integration of equation (3), those with dashed lines represent expansion equation (34) with terms up to second order, and the dotted lines the same expression but with terms of third order. For these values we obtain from equation (37) intervals $0.0116 \leqslant a/d \leqslant 0.0970$ and $0.0116 \leqslant a/d \leqslant 0.0972$ for prograde and retrograde orbits, respectively. The results of numerical integration of the exact expressions are depicted in Figs 6(a)–(c) with parameter values $m/d = 0.15$, $\alpha/d = 0.05$, $a/d = 0.175$ in Fig. 6(a), $a/d = 0.225$ in Fig. 6(b) and $a/d = 0.275$ in Fig. 6(c). The values for prograde orbits are represented by dashed lines, retrograde orbits by dotted lines, and solid lines the perihelion shift without rotation (Weyl disc). We note that for prograde orbits the Kerr parameter lowers the angle of precession and has an opposite effect for retrograde orbits. The signs in the expansion equation (34) also predict these effects.

Finally in Figs 7(a) and (b) the parameters $m/d = 0.15$ and $a/d = 0.225$ were held constant and the Kerr parameter was changed: $\alpha/d = 0$ (solid lines), $\alpha/d = 0.05$ (dashed lines) and $\alpha/d = 0.1$ (dotted lines). Prograde orbits are shown in Fig. 7(a) and retrograde orbits in (b). Rotation has the same effect on both types of orbits as observed in Fig. 6.

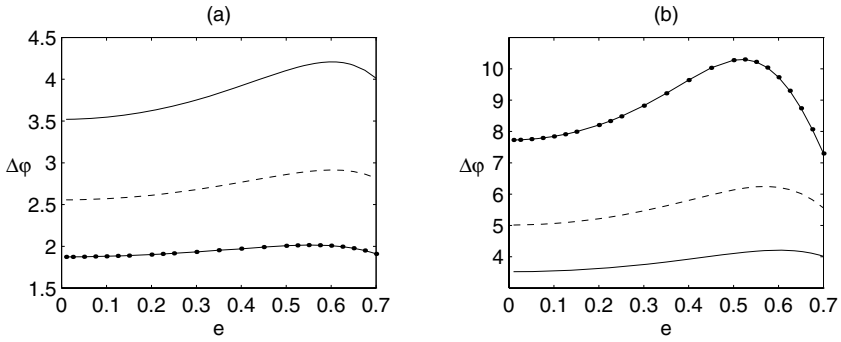

Figure 7. The perihelion shift $\Delta\varphi$ as function of excentricity e for the Kerr disc: (a) prograde orbits and (b) retrograde orbits. Parameters: $m/d = 0.15$, $a/d = 0.225$, $\alpha/d = 0$ (solid lines), $\alpha/d = 0.05$ (dashed lines) and $\alpha/d = 0.1$ (dotted lines).

5 EFFECT OF NEWTONIAN PRECESSION

The advance of perihelion calculated for the relativistic models of discs presented in Sections 3 and 4 has two origins: one due to relativity and other from purely Newtonian gravity, since any flattened body will generate a perihelion precession. Thus, it would be interesting to separate the relativistic from the Newtonian contributions to the precession.

It can be shown that in the non-relativistic limit the above mentioned disc models reduce on the $z = 0$ plane to the Kuzmin model (Kuzmin 1956):

$$\Phi = -\frac{m}{\sqrt{r^2 + a^2}}. \tag{38}$$

The orbital equation in the usual cylindrical coordinates reads

$$\frac{\mathrm{d}r}{\mathrm{d}\varphi} = r\left[\frac{2r^2(E_\mathrm{M} - \Phi)}{h^2} - 1\right]^{1/2}, \tag{39}$$

where E_M is the conserved mechanical energy of the test particle

$$E_\mathrm{M} = \frac{r_\mathrm{p}^2\Phi_\mathrm{p} - r_\mathrm{m}^2\Phi_\mathrm{m}}{r_\mathrm{p}^2 - r_\mathrm{m}^2}, \quad \text{and} \qquad h = \frac{2r_\mathrm{p}^2 r_\mathrm{m}^2(\Phi_\mathrm{p} - \Phi_\mathrm{m})}{r_\mathrm{p}^2 - r_\mathrm{m}^2}, \tag{40}$$

with the notation as defined in Section 3.1. Proceeding as in the previous sections, it is possible to deduce approximate expressions for the perihelion shift. Using equations (3) and (38)–(40), one has the following expansion:

$$\Delta\varphi = -\frac{3\pi a^2}{d^2(1 - e^2)^2} + \mathcal{O}((a/d)^4). \tag{41}$$

Note that the angle of advance is independent of m, which is cancelled in the fraction in equation (39). Thus, the first term of equation (41), which also appears in expansions (14), (15), (24) and (34), is the purely Newtonian contribution up to third order to the perihelion shift.

As a numerical example, in Figs 8(a)–(c) we display curves of $\Delta\varphi$ as function of the excentricity e for the Schwarzschild disc in isotropic coordinates with $m/d = 0.01$, $a/d = 0.175$ in Fig. 8(a), $a/d = 0.225$ in Fig. 8(b) and $a/d = 0.275$ in Fig. 8(c); the same values that were used in Fig. 4. The solid lines represent the total angle of precession; the dotted lines represent the precession due to Newtonian effects obtained from the numerical integration of equation (3) with equations (38)–(40), and the dashed lines are the difference between the previous two values. It is seen that the precession rate due to Newtonian gravity is in the opposite sense to the relativistic precession. Also for less relativistic discs the Newtonian contribution is more significant, as expected.

6 DISCUSSION

We studied the advance of perihelion for elliptic orbits of test particles in geodesic motion on the galactic plane for relativistic static and stationary disc models. We derived approximate expressions for the perihelion shift and compared them with the numerical integration of the exact solutions. The results show that the angle of advance can increase as well as decrease with increasing excentricity. We have that highly relativistic discs favours the first situation, and the advance of perihelion decreases with excentricity when the discs become less relativistic. The effect of rotation was also studied for a particular stationary disc model based on the Kerr solution. We found that the Kerr parameter lowers the perihelion shift for prograde orbits and increases it in the case of retrograde orbits. We also calculated the different contributions (Newtonian and relativistic) to the advance of perihelion for the relativistic disc models.

Our conclusions are based on the study of a few exact general relativistic disc models, in particular, the Miyamoto–Nagai model, that presents some characteristics of real galaxies. We believe that the results found may be common to other models of galaxies.

ACKNOWLEDGMENTS

We thank FAPESP for financial support. PSL also thanks CNPq.

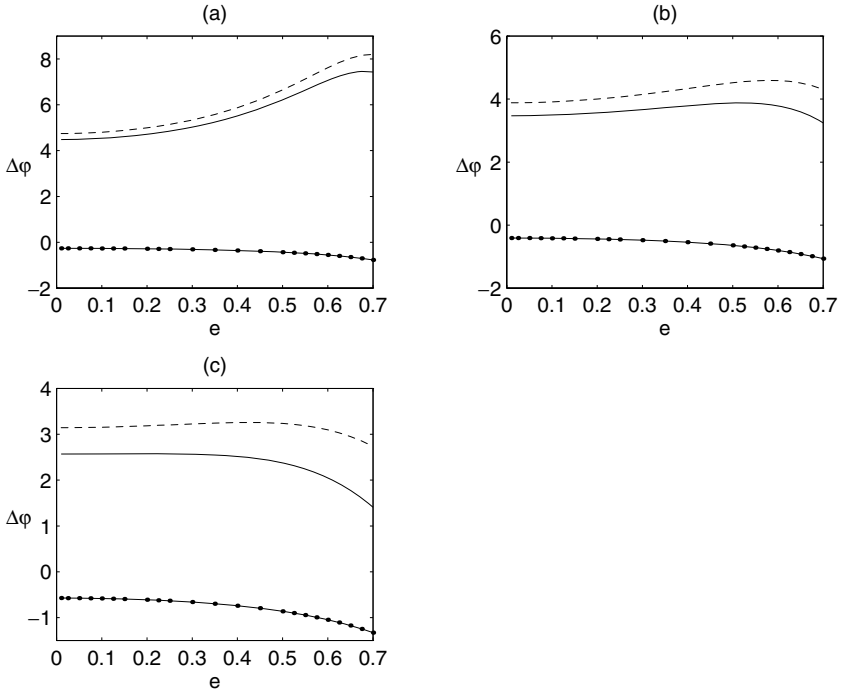

Figure 8. The different contributions to the perihelion shift $\Delta\varphi$ as function of excentricity e for the Schwarzschild disc in isotropic coordinates. Parameters: $m/d = 0.15$, $a/d = 0.175$ in (a), $a/d = 0.225$ in (b) and $a/d = 0.275$ in (c). Solid lines: the total shift. Dotted lines: the purely Newtonian contribution. Dashed lines: the relativistic contribution.

REFERENCES

Bardeen J. M., Wagoner R. V., 1971, ApJ, 167, 359
Bičák J., Ledvinka T., 1993, Phys. Rev. Lett., 71, 1669
Bičák J., Lynden-Bell D., Katz J., 1993a, Phys. Rev. D, 47, 4334
Bičák J., Lynden-Bell D., Pichon C., 1993b, MNRAS, 265, 126
Bini D., De Paolis F., Geralico A., Ingrosso G., Nucita A., 2005, Gen. Relativ. Gravit., 37, 1263
Boisseau B., Letelier P. S., 2002, Gen. Relativ. Gravit., 34, 1077
Chamorro A., Gregory R., Stewart J. M., 1987, Proc. R. Soc. A, 413, 251
Chazy M., 1924, Bull. Soc. Math. France, 52, 17
Curzon H., 1924, Proc. London Math. Soc., 23, 477
González G., Espitia O. A., 2003, Phys. Rev. D, 68, 104028
González G., Letelier P. S., 2000, Phys. Rev. D, 62, 064025
González G., Letelier P. S., 2004, Phys. Rev. D, 69, 044013
Hulse R. A., Taylor J. H., 1975, ApJ, 195, L51
Kuzmin G. G., 1956, Astron. Zh., 33, 27
Lemos J. P. S., 1989, Class. Quantum Gravity, 6, 1219
Lemos J. P. S., Letelier P. S., 1994, Phys. Rev. D, 49, 5135
Lynden-Bell D., Pineault S., 1978, MNRAS, 185, 679
Miyamoto M., Nagai R., 1975, PASJ, 27, 533
Morgan T., Morgan L., 1969, Phys. Rev., 183, 1097
Neugebauer G., Meinel R., 1995, Phys. Rev. Lett., 75, 3046
Pichon C., Lynden-Bell D., 1996, MNRAS, 280, 1007
Schäfer G., Damour T., 1988, Nuovo Cimento B, 101, 127
Schäfer G., Wex N., 1993, Phys. Lett. A, 174, 196
Vogt D., Letelier P. S., 2003, Phys. Rev. D, 68, 084010
Vogt D., Letelier P. S., 2005a, Phys. Rev. D, 71, 084030
Vogt D., Letelier P. S., 2005b, MNRAS, 363, 268
Vogt D., Letelier P. S., 2007, Phys. Rev. D, 76, 084010
Weyl H., 1917, Ann. Phys., 54, 117
Weyl H., 1919, Ann. Phys., 59, 185

This paper has been typeset from a TEX/LATEX file prepared by the author.